

2025 | 440

## Fuel slip monitoring in high-humidity flue gases from co-firing of ammonia with methane

Controls, Automation, Measurement, Monitoring & Predictive Maintenance

**Liuhaio Ma, Wuhan University of Technology**

Hao Wang, Wuhan University of Technology  
Wei Wang, Wuhan University of Technology  
Yu Wang, Wuhan University of Technology

---

This paper has been presented and published at the 31st CIMAC World Congress 2025 in Zürich, Switzerland. The CIMAC Congress is held every three years, each time in a different member country. The Congress program centres around the presentation of Technical Papers on engine research and development, application engineering on the original equipment side and engine operation and maintenance on the end-user side. The themes of the 2025 event included Digitalization & Connectivity for different applications, System Integration & Hybridization, Electrification & Fuel Cells Development, Emission Reduction Technologies, Conventional and New Fuels, Dual Fuel Engines, Lubricants, Product Development of Gas and Diesel Engines, Components & Tribology, Turbochargers, Controls & Automation, Engine Thermodynamics, Simulation Technologies as well as Basic Research & Advanced Engineering. The copyright of this paper is with CIMAC. For further information please visit <https://www.cimac.com>.

## ABSTRACT

Ammonia (NH<sub>3</sub>) has been recently recognized as promising carbon-free future fuel towards decarbonizing both the power and industrial heating sectors. The past five years have seen rapid development and demonstration in co-firing of ammonia with methane for applications in engines, gas turbines, thermal power plants and industrial furnaces. However, fuel slip is of high concern because of the low reactivity and high toxicity of NH<sub>3</sub> and strong greenhouse effect of CH<sub>4</sub>, motivating the development of sensitive sensor for real-time monitoring of fuel emissions in combustion flue gases. In this work, a near-infrared absorption spectroscopic sensor was developed for trace NH<sub>3</sub> and CH<sub>4</sub> measurements in high-temperature flue gas environments with water vapor (H<sub>2</sub>O) concentration as high as 50% (mole fraction), which is particularly suitable for monitoring fuel slip in ammonia-methane combustion system. The sensor used a distributed feedback (DFB) laser to target the NH<sub>3</sub> absorption line near 6612.73 cm<sup>-1</sup> and CH<sub>4</sub> near 6046.95 cm<sup>-1</sup>. Proof-of-concept tests were conducted in a high-temperature multi-pass cell with a controlled temperature of 500 K and pressure of 1 atm. A custom-designed variable humidity generator was used to provide reference NH<sub>3</sub>/CH<sub>4</sub>/N<sub>2</sub> mixture with controlled H<sub>2</sub>O concentration (10%-40%) to simulate combustion flue gases. Direct absorption spectroscopy (DAS) and wavelength modulation spectroscopy (WMS) were both used to ensure a relatively large dynamic range. H<sub>2</sub>O-induced broadening effects on the measured absorption profile were quantified. The developed sensor was firstly validated against NH<sub>3</sub>/CH<sub>4</sub>/N<sub>2</sub> mixtures with different H<sub>2</sub>O concentrations with a lower detection limit of 0.1 ppm achieved. Real-time measurement of fuel slip in the flue gases from CH<sub>4</sub>/NH<sub>3</sub>/air flames were performed as a demonstration of the sensor for time-resolved fuel monitoring with sufficient accuracy, sensitivity, and time response.

## 1. Introduction

Laser spectroscopic techniques offer significant advantages, such as high sensitivity, selectivity, rapid response, and excellent quantification capabilities, and have been widely applied in environmental monitoring, hazardous chemical identification, combustion diagnostics, and pollutant emission analysis [1–4]. With the “carbon peak and carbon neutrality” strategy now incorporated into the overall framework of ecological civilization, the energy sector faces unprecedented challenges, making the deep decarbonization of conventional energy systems a critical task across various industries. Recent fundamental research and engineering practice have demonstrated that blending methane with ammonia to form a dual-fuel mixture can reduce CO<sub>2</sub> emissions during combustion while compensating for the poor flammability and flame stability of pure ammonia fuels. However, incomplete mixing of the dual fuel with air may result in suboptimal combustion dynamics and local flame extinction, thereby exacerbating the issue of trace-level fuel leakage. Moreover, excessive ammonia injection in denitrification systems further aggravates ammonia slip. Large-scale emissions of ammonia (NH<sub>3</sub>) can cause soil alkalization and water eutrophication, and as an alkaline gas, NH<sub>3</sub> readily reacts with atmospheric nitrogen oxides to form aerosols that are directly associated with PM<sub>2.5</sub> pollution [5]. Additionally, methane (CH<sub>4</sub>), a typical greenhouse gas, exerts a significant impact on global climate change. Therefore, strict regulation of trace fuel leakage during dual-fuel combustion is imperative to ensure compliance with environmental standards, and precise detection of such leakage is critical for evaluating combustion efficiency.

In response to the need for high-sensitivity detection of trace methane and ammonia at elevated temperatures, several mature and reliable spectroscopic gas detection techniques have been developed, including non-dispersive

infrared/ultraviolet (NDIR/NDUV) methods, Fourier transform infrared (FTIR) spectroscopy, and laser absorption spectroscopy (LAS). The NDIR technique [6] deduces target gas concentrations by analyzing the broadband infrared absorption spectra of gas molecules. This method is relatively cost-effective and can be applied to various gases exhibiting infrared absorption features. However, the presence of water vapor interference significantly degrades measurement accuracy when detecting trace ammonia. FTIR spectroscopy [7], combined with heated high-temperature gas cells, enables rapid analysis of trace gases. Although FTIR offers improved performance compared to NDIR, water vapor spectral interference remains a challenge, and the bulky, high-cost instrumentation limits its applicability. Non-dispersive ultraviolet (NDUV) techniques [8] address water interference by shifting measurements into the ultraviolet spectral region, where water vapor absorption is negligible; however, under harsh conditions, fluctuations in UV light intensity can compromise measurement accuracy. It is also noteworthy that moisture removal by condensation—a common practice in commercial gas analyzers—is not feasible for ammonia measurements due to its high solubility in water. Furthermore, most of these sensor technologies require frequent calibration, a process that can be cumbersome for continuous flue gas monitoring. In addition to spectral cross-interference from water vapor, high water vapor concentrations can induce significant broadening of methane and ammonia absorption lines, thereby reducing measurement accuracy and reliability [9].

Over the past several decades, laser absorption spectroscopy (LAS) has attracted extensive attention in the field of trace gas detection due to its high sensitivity, rapid response, robustness, accuracy, compactness, and selectivity [10]. Frequency division multiplexing (FDM) technology enables the simultaneous coupling of multiple lasers at distinct wavelengths, permitting individual modulation and demodulation of each laser signal

while preserving temporal resolution. When combined with LAS, this approach facilitates rapid and precise quantification of multi-component gas concentrations. High-temperature trace methane and ammonia detection systems based on LAS have been successfully demonstrated in various experimental and industrial applications. Notably, Ma et al. [9] were the first to design a sensor capable of measuring trace  $\text{NH}_3$  concentrations in high-temperature, high-humidity environments, systematically investigating the influence of water vapor concentration near 1512 nm on  $\text{NH}_3$  absorption and achieving accurate detection of ammonia slip under humid conditions. Duan et al. [11] developed a calibration-free wavelength modulation spectroscopy-based sensor for simultaneous NO and  $\text{NH}_3$  detection, attaining low detection limits for both species. Guo et al. [12] utilized time division multiplexing to couple multiple lasers, enabling concurrent detection of  $\text{NH}_3$ , NO, and temperature, and later introduced a machine learning approach to denoise the absorption signals and improve the signal-to-noise ratio [13]. Li et al. [14] used a single laser covering  $\text{NH}_3$  absorption at  $6612.73\text{ cm}^{-1}$  and  $\text{H}_2\text{O}$  absorption at  $6612.03\text{ cm}^{-1}$  and  $6609.85\text{ cm}^{-1}$  to simultaneously measure ammonia, temperature, and water vapor concentration. Guo et al. [15] also developed a portable integrated  $\text{NH}_3$  sensor, with quantitative analysis indicating that ammonia adsorption is significantly suppressed at temperatures of 415 K or higher, thereby enhancing sensing accuracy at elevated temperatures. These studies demonstrate that while wavelength modulation spectroscopy has been widely applied in high-temperature or multi-species and multi-parameter sensing, research on multi-species detection under high-temperature and high-humidity conditions remains relatively scarce.

In the present study, we combine frequency division multiplexing with normalized wavelength modulation spectroscopy to couple two lasers with central wavelengths of 1512 nm and 1654 nm, thereby developing a synchronous measurement

system for  $\text{NH}_3$  and  $\text{CH}_4$  under high-temperature, high-humidity conditions. This system is specifically designed for the quantitative detection of trace  $\text{NH}_3$  and  $\text{CH}_4$  in humid flue gas environments. A multi-line fitting method is employed to accurately determine water vapor concentration. By designing a mixed gas system that simulates trace-level methane and ammonia under high water vapor backgrounds, we obtained harmonic signals for  $\text{NH}_3/\text{CH}_4$  in the concentration range of 1ppm to 100ppm within water vapor concentrations ranging from 10% to 50%, thereby quantifying the influence of water vapor on the harmonic signals. Furthermore, the reliability of the system was verified by comparing the FDM-based measurement results with those obtained from single-channel measurements. The detection system exhibits excellent linearity for trace dual-fuel concentrations between 1ppm and 100ppm, with detection limits of 82ppb for  $\text{CH}_4$  at an integration time of 92 s and 88ppb for  $\text{NH}_3$  at an integration time of 40 s.

## 2. Experimental system

### 2.1 Optimal selection of absorption lines

For achieving high-sensitivity detection of the target gases, the careful selection of appropriate absorption lines is of paramount importance. In the context of trace dual-fuel leakage during methane-doped ammonia combustion, it is essential first to avoid spectral interference from the primary combustion products (namely, water vapor ( $\text{H}_2\text{O}$ ) and carbon dioxide ( $\text{CO}_2$ )) as well as from pollutants (such as carbon monoxide (CO) and nitric oxide (NO)). Secondly, sufficiently strong absorption lines must be selected to enable high-sensitivity detection. Although the fundamental absorption bands in the mid-infrared offer robust absorption features, the associated interband cascade lasers, quantum cascade lasers, and their respective controllers and photodetectors are prohibitively expensive, limiting their scalability for online industrial flue gas monitoring. In contrast, advancements in optical communication

technology have led to the maturity of near-infrared lasers and detectors. When combined with fiber-delivered light and compact multipass gas absorption cells, these systems can achieve high-sensitivity detection at a significantly lower cost.

Figure 1(a) illustrates the spectral line intensity distributions of  $\text{NH}_3$  and  $\text{CH}_4$ , along with those of  $\text{H}_2\text{O}$ ,  $\text{CO}$ ,  $\text{CO}_2$ , and  $\text{NO}$ , within the 1–3  $\mu\text{m}$  wavelength range at 473.15 K. It is evident that  $\text{NH}_3$  and  $\text{CH}_4$  exhibit excellent spectral isolation from the other gas components within the 1.5–1.7  $\mu\text{m}$  range. Based on spectral analysis, the absorption lines for  $\text{NH}_3$  and  $\text{CH}_4$  at  $6612.73\text{ cm}^{-1}$  and  $6046.95\text{ cm}^{-1}$ , respectively, were selected because the spectral features of these target species in the vicinity of these wavenumbers are minimally affected by interference from  $\text{CO}$ ,  $\text{CO}_2$ , and  $\text{NO}$ . Figure 1(b) and 1(c) demonstrate that as the  $\text{H}_2\text{O}$  concentration

increases from 10% to 50%, the spectral analysis of  $\text{NH}_3$  becomes increasingly challenging due to water vapor interference, thereby complicating the measurement of  $\text{NH}_3$  concentration. In contrast, the  $\text{CH}_4$  absorption features near 1.65  $\mu\text{m}$  are less susceptible to the influence of  $\text{H}_2\text{O}$ . It is noteworthy that our previous spectral simulation studies revealed that even the widely used mid-infrared  $\text{NH}_3$  absorption lines cannot fully mitigate the effects of high water vapor interference [15]. Although the absorption characteristics of  $\text{NH}_3$  are affected by water vapor, employing a 1512 nm laser to simultaneously scan the absorption lines of  $\text{H}_2\text{O}$  and  $\text{NH}_3$  enables the assessment of interference by quantifying the  $\text{H}_2\text{O}$  concentration, thus facilitating sensor performance optimization. Consequently, the absorption lines at  $6046.95\text{ cm}^{-1}$  and  $6612.73\text{ cm}^{-1}$  were ultimately chosen for the detection of  $\text{CH}_4$  and  $\text{NH}_3$ , respectively.

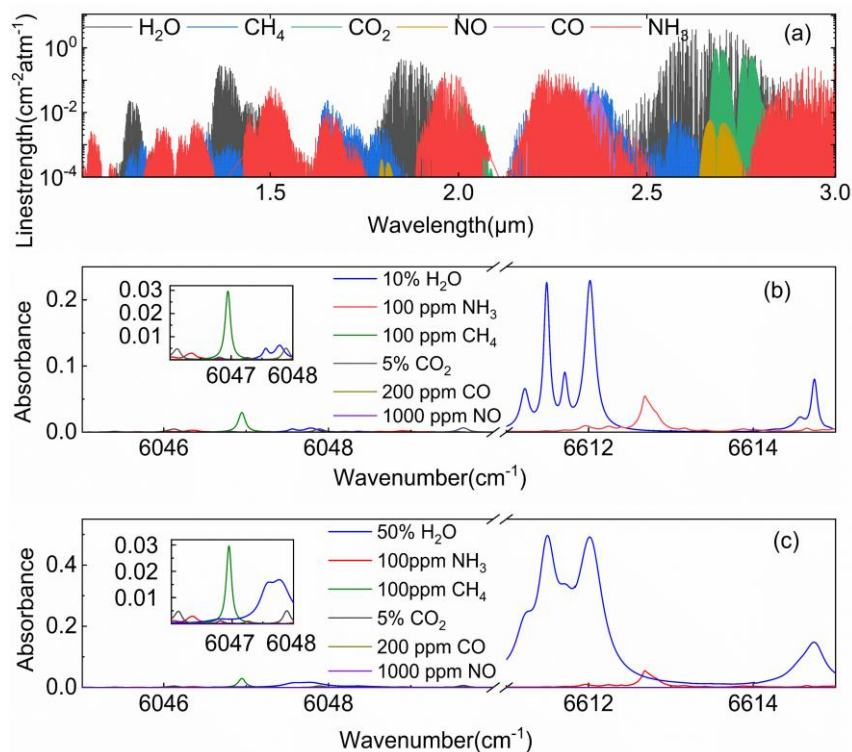


Figure 1. (a) Line intensities of  $\text{NH}_3$ ,  $\text{CH}_4$ ,  $\text{CO}_2$ ,  $\text{NO}$ ,  $\text{CO}$  and  $\text{H}_2\text{O}$  in 1–3 $\mu\text{m}$ ; (b–c) Simulated absorbance of 10%  $\text{H}_2\text{O}$  and 50%  $\text{H}_2\text{O}$ , 100 ppm  $\text{NH}_3$  and 100 ppm  $\text{CH}_4$  at 473 K based on Hitran2020 database

## 2.2 Optical setup

Figure 2 illustrates the experimental system for

high-humidity trace dual-fuel measurements, which comprises two primary subsystems: a high-humidity trace mixed-gas configuration module (left dashed box) and a laser absorption

spectroscopy measurement module (right dashed box). Experiments were conducted at atmospheric pressure, and precise target gas concentrations were achieved by finely adjusting the mass flow controllers (D07, Qixing Huachuang) to regulate the flow rates of trace  $\text{CH}_4/\text{N}_2$  standard gas, trace  $\text{NH}_3/\text{N}_2$  standard gas, and  $\text{N}_2$ . Nitrogen was supplied in two separate streams: one served as the carrier gas to the nebulizer (TR-50-K2, Meinhard) for atomizing distilled water delivered via an injection pump (LSP01-3A, Longer), while the other acted as a diluent to establish a high-humidity background (with  $\text{H}_2\text{O}$  concentrations ranging from 10% to 50%) for mixing the target gases at trace levels (1ppm–100ppm). To prevent condensation of the nebulized water vapor—which could dissolve ammonia—a high-temperature heating tape was wrapped around the gas delivery lines, and both the high-temperature gas cell and the heating tape were maintained at 473 K to ensure complete vaporization of the distilled water. Under these conditions, water and ammonia remain in the gaseous state, and the mixture of trace ammonia, water vapor, and nitrogen does not form ammonium hydroxide, thereby eliminating potential interference in the detection of trace  $\text{NH}_3$ .

To achieve synchronous measurements of  $\text{H}_2\text{O}$ , trace  $\text{CH}_4$ , and  $\text{NH}_3$  under high-humidity conditions, two lasers with central wavelengths of 1512 nm and 1654 nm (EP1512-DM-B06-FA and EP1654-DM-B06-FA, Eblana) were employed. These lasers cover the spectral features of  $\text{H}_2\text{O}$  at  $6612.03\text{ cm}^{-1}$ ,  $\text{NH}_3$  at  $6612.73\text{ cm}^{-1}$ , and  $\text{CH}_4$  at  $6046.95\text{ cm}^{-1}$ , respectively. The temperature and

injection current of the lasers were precisely controlled using low-noise commercial laser controllers (LDTC5020 and M01). A LabVIEW-based program was utilized to generate the required modulation signals for both direct absorption spectroscopy (DAS) and wavelength modulation spectroscopy (WMS); this program superimposed sine-wave modulation onto a triangular scanning signal. In the experiments, both lasers were modulated with a 10 Hz triangular scan, while sine-wave modulation signals at 15 kHz and 11 kHz were applied to the 1512 nm and 1654 nm lasers, respectively, to facilitate subsequent signal demodulation. The two laser beams were combined via a fiber beam combiner (HJFT-FBT, Hangjia Optoelectronics) and directed into a high-temperature, multipass White-type gas cell. Within the gas cell, multiple reflections yielded an effective absorption path length of 1800 cm. Upon exiting the cell, the laser beam was focused by a convex lens onto the active area of an indium gallium arsenide photodetector (PDA20CS2, Thorlabs), and the resulting signal was transmitted via a BNC cable to a data acquisition card (USB6363, NI). Additionally, to mitigate  $\text{NH}_3$  adsorption on the cell walls, the interior of the high-temperature gas cell was coated with polytetrafluoroethylene, and measurements were conducted under continuous flow conditions. The core hardware of the experimental system—including the 16-bit data acquisition card, high-precision laser controllers, and low-noise photodetectors—is of high quality, effectively preventing data degradation due to hardware limitations.

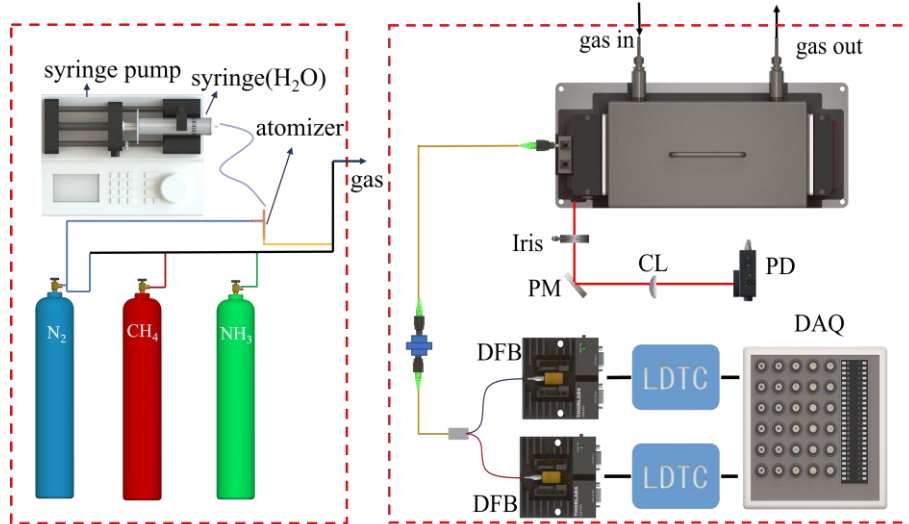


Figure 2. Experimental system for trace NH<sub>3</sub>/CH<sub>4</sub> measurements under high-temperature, high-humidity conditions

### 3. Results and discussions

#### 3.1 Measurement of Water Vapor Concentration in a High-Humidity Environment

In this study, the accurate configuration of a high-humidity environment is essential for sensor development, validation, and calibration. The required injection pump feed rate for generating the high-temperature, high-humidity gas mixture was determined based on mass conservation principles and the ideal gas law [15]. The configuration procedure is as follows:

First, the total gas flow rate at high temperature is established. In the experiment, the total flow rate was set to 5000 mL/min at 473 K. From the total flow rate, the volume flow rate of water vapor at the designated temperature and water concentration is calculated, and subsequently, the liquid water flow rate is determined according to Equation (1):

$$Q_{H_2O} = \frac{V_{H_2O}' \cdot M_{H_2O}' \cdot 273.15}{22.4' \cdot 1000' \cdot r_{H_2O}' \cdot T_1} \quad (1)$$

Here,  $Q$  denotes the liquid water flow rate (mL/min),  $\rho_{H_2O}$  represents the density of liquid water (g/mL), and  $M_{H_2O}$  is the molecular weight of water (g/mol). Secondly, based on the total gas flow rate, the target gas concentration, and the

concentrations of the CH<sub>4</sub>/N<sub>2</sub> and NH<sub>3</sub>/N<sub>2</sub> standard gases, the high-temperature volume flow rate of the standard gas can be calculated; then, using Equation (2), the standard gas volume flow rate at room temperature can be determined.

$$V_0 = V_1' \cdot \frac{T_0}{T_1} \quad (2)$$

Here,  $V_0$  represents the gas volumetric flow rate at room temperature (mL/min),  $V_1$  is the gas volumetric flow rate at the set temperature (mL/min),  $T_0$  denotes the room temperature (K), and  $T_1$  corresponds to the designated temperature (K).

To verify the accuracy of the high-humidity configuration, the water concentration was determined by measuring the integrated absorbance near 1512 nm using direct absorption spectroscopy (DAS). Figure 3(a) displays the raw absorption spectrum obtained at a 10% H<sub>2</sub>O concentration, where the weak baseline absorption is attributed to the minimal water vapor present in ambient air at room temperature. Figure 3(b) presents the typical absorbance signals, along with the Voigt fitting results and corresponding fitting residuals, for water vapor concentrations of 10% and 50%. Figure 3(c) compares the configured water concentrations with the actual measured

values. In this comparison, the vertical error bars represent the uncertainty of the DAS measurements (approximately 4.0%), while the horizontal error bars indicate the uncertainty in the high-temperature water vapor configuration (approximately 2.2%). Across the range of five water concentrations from 10% to 50%, the measured values closely match the configured values, with a maximum error of 3.5%, which is within acceptable limits. These results confirm the reliability of the high-humidity environment configuration system.

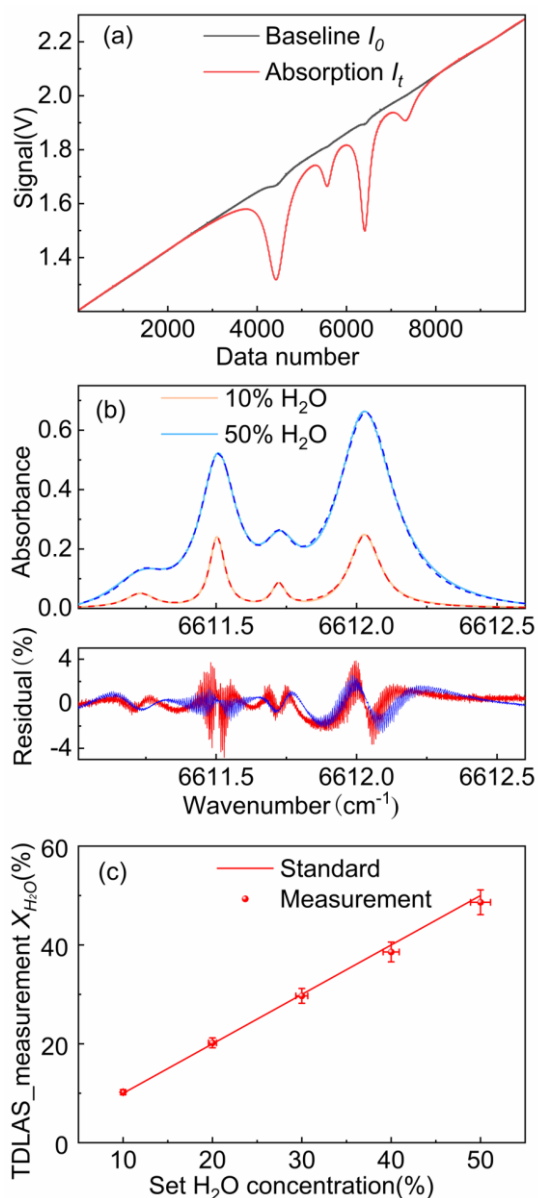


**Figure 3.** (a) Raw signal from direct absorption of measured H<sub>2</sub>O concentration; (b) Voigt fit curve for 10%-50% H<sub>2</sub>O concentration; (c) Comparison of set H<sub>2</sub>O concentration and experimental H<sub>2</sub>O concentration

### 3.2 Detection of trace NH<sub>3</sub>/CH<sub>4</sub> concentration in high temperature and high humidity environments

Figures 4(a) and 4(b) present the raw WMS signals for individual measurements of 100ppmNH<sub>3</sub> and 100ppm CH<sub>4</sub> in a 30% H<sub>2</sub>O environment. Figure 4(c) shows the raw WMS signals obtained using frequency division multiplexing to simultaneously measure CH<sub>4</sub> and NH<sub>3</sub> under the same conditions; the overall decrease in voltage is attributed to a reduction in the amplification gain of the photodetector (PD). It is observed that the raw WMS signals for the two gases exhibit a periodic variation, with the voltage amplitude rising and subsequently falling within each cycle. This behavior results from the differing high-frequency modulation frequencies applied to each gas signal prior to modulation, which leads to alternating additive and subtractive effects when the signals are superimposed. Figures 4(d) and 4(e) display the WMS-2f/1f signals for various concentrations of NH<sub>3</sub> and CH<sub>4</sub>, demodulated based on their respective modulation frequencies during simultaneous measurements in a 30% H<sub>2</sub>O environment. Notably, even under high-humidity conditions, the detection limits for NH<sub>3</sub> and CH<sub>4</sub> remain at 10ppm and 2ppm, respectively, underscoring the sensor's exceptional sensitivity.



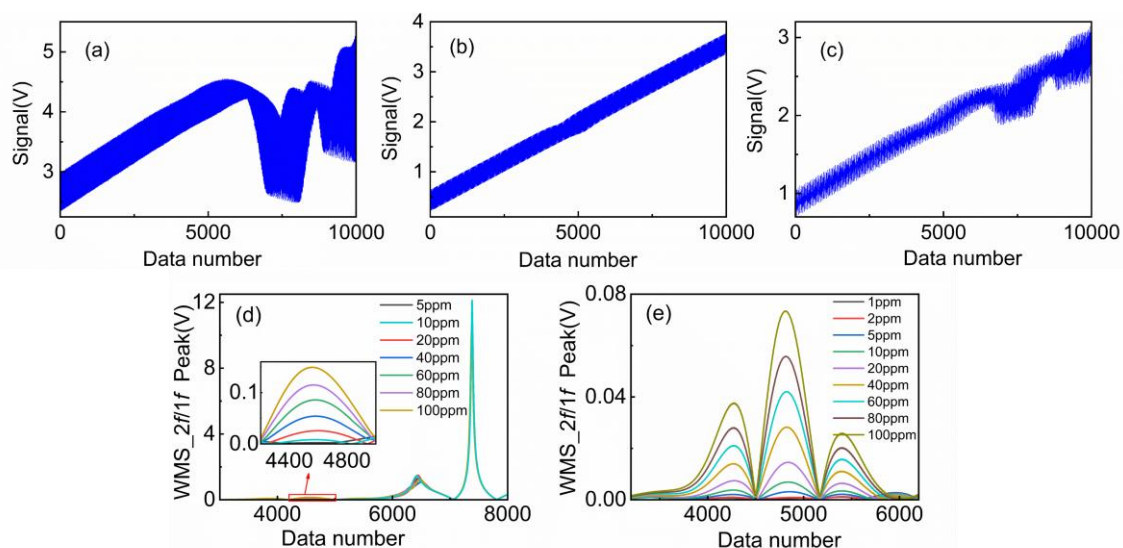


**Figure 4.** (a-c) Raw WMS signals of 100 ppm NH<sub>3</sub>, 100 ppm CH<sub>4</sub>, and co-measurements of 100 ppm NH<sub>3</sub>, 100 ppm CH<sub>4</sub> measured individually and co-measurements in 30% H<sub>2</sub>O environment; (d-e) NH<sub>3</sub>/CH<sub>4</sub> WMS-2f/1f curves of different concentrations when measured co-measurements are made in 30% H<sub>2</sub>O environment

To comprehensively evaluate the synchronous detection performance of the sensor and assess the influence of high humidity on the WMS-2f/1f

signals, this study compared the simultaneous measurement signals of CH<sub>4</sub> and NH<sub>3</sub> with those obtained from independent measurements under varying H<sub>2</sub>O concentrations. Initially, independent measurements of NH<sub>3</sub> and CH<sub>4</sub> were conducted in a high-humidity environment to establish baseline data. Figures 5(a) and 5(b) display the WMS-2f/1f peak curves for individually measured NH<sub>3</sub> and CH<sub>4</sub> (with concentrations ranging from 1 ppm to 100 ppm) at H<sub>2</sub>O concentrations between 10% and 50%. These data reflect the absorption characteristics of the individual gases under different humidity conditions and serve as reference standards. Figures 5(c) and 5(d) present the WMS-2f/1f peak curves for the simultaneous detection of NH<sub>3</sub> and CH<sub>4</sub> (within the same concentration range) under identical H<sub>2</sub>O concentration conditions. By plotting the WMS-2f/1f peak amplitudes as a function of gas concentration and fitting the data, the resulting linearity (with  $R^2$  values exceeding 0.997) confirms that both the independent and simultaneous

measurement curves exhibit excellent linear responses, thereby demonstrating the sensor's outstanding linearity.

Analysis of the measurement signals indicates that, regardless of whether the gases are measured individually or simultaneously, the WMS-2f/1f peak signals for both NH<sub>3</sub> and CH<sub>4</sub> decrease as the H<sub>2</sub>O concentration increases from 0% to 50%. Under synchronous measurement conditions, the WMS-2f/1f peak signal for NH<sub>3</sub> decreased by approximately 36%–38% at 50% H<sub>2</sub>O relative to 0% H<sub>2</sub>O, while that for CH<sub>4</sub> decreased by about 20%–25%. The more pronounced reduction in the NH<sub>3</sub> signal is primarily attributable to the broadening effect induced by high water vapor, which significantly enhances collisional broadening of NH<sub>3</sub> relative to CH<sub>4</sub>, thereby reducing the peak absorbance. It is noteworthy that, in addition to the broadening effect, the selected NH<sub>3</sub> absorption feature is subject to interference from baseline elevation near 6612.01 cm<sup>-1</sup> under high water vapor conditions, and similarly, the chosen CH<sub>4</sub> absorption feature is affected by baseline elevation near 6047.79 cm<sup>-1</sup>. Although such interference would tend to increase the signal, the observed decrease in the harmonic signal clearly indicates

that the broadening effect is dominant. Moreover, since water vapor influences the two target gas molecules differently— $\text{NH}_3$ , with its higher broadening coefficient, is more strongly affected than  $\text{CH}_4$ —the water vapor broadening effect significantly degrades the detection limit for  $\text{NH}_3$ , and this degradation intensifies with increasing  $\text{H}_2\text{O}$  concentration. Specifically, at  $\text{H}_2\text{O}$  concentrations of 10%, 30%, and 50%, the detection limits for  $\text{NH}_3$  increased from 1ppm to 5ppm and 20ppm, respectively, exhibiting a clear upward trend. In contrast, for  $\text{CH}_4$ , the detection limit remained at 1ppm for  $\text{H}_2\text{O}$  concentrations below 30%, and even at 50%  $\text{H}_2\text{O}$ , a low detection

limit of 5ppm was maintained. A comparison between the results of simultaneous and independent measurements revealed that the demodulated synchronous measurement signals obtained via frequency division multiplexing are essentially identical to the individually demodulated signals of  $\text{CH}_4$  and  $\text{NH}_3$ , with both maintaining excellent linearity. These findings confirm that the developed trace dual-fuel sensor for simultaneous detection is capable of meeting practical measurement requirements, offering high accuracy and significant practical value for real-world applications.

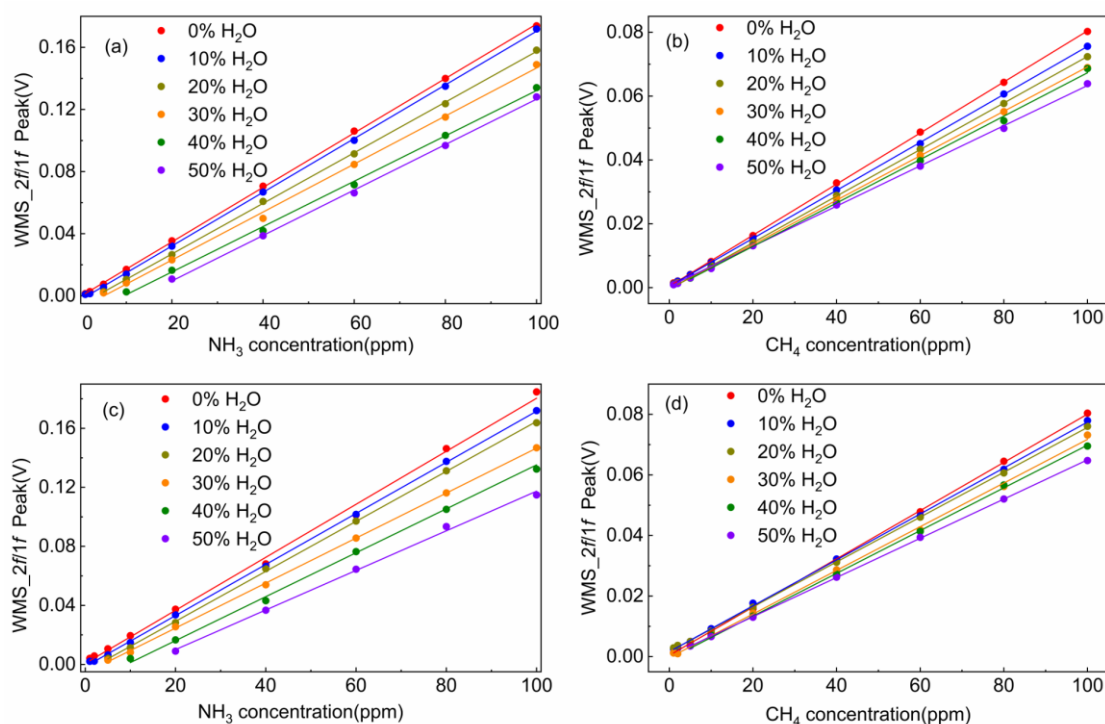


**Figure 5.** (a-b)  $\text{NH}_3/\text{CH}_4$  WMS-2f/1f peak signals during standalone measurements; (c-d)  $\text{NH}_3/\text{CH}_4$  WMS-2f/1f peak signals during frequency-division multiplexing measurements.

For WMS measurements, the Allan-Werle variance was employed to analyze the system noise level, assess the sensor's long-term stability, and determine the minimum detection limits. Figure 6 presents the Allan variance for a continuous 1800 s measurement, from which the detection limits for  $\text{NH}_3$  and  $\text{CH}_4$  were found to be approximately 82ppb and 88ppb, respectively, with integration times of 91 s and 40 s. On a 1 s timescale, the detection limits for  $\text{NH}_3$  and  $\text{CH}_4$  are 0.44ppm and

0.81ppm, respectively.

To further evaluate the performance of the trace  $\text{CH}_4/\text{NH}_3$  simultaneous detection sensor, a series of experiments were designed. A gas mixture of  $\text{H}_2\text{O}$ ,  $\text{CH}_4$ ,  $\text{NH}_3$ , and  $\text{N}_2$  was introduced into the high-temperature gas cell of the experimental system. The concentrations of  $\text{CH}_4$  and  $\text{NH}_3$  were continuously adjusted while monitoring the sensor's response, and the measured signals were converted into corresponding concentration values

for real-time monitoring. The experimental results indicate that the sensor rapidly responds to changes in gas concentration and maintains excellent stability during long-term continuous operation. Figure 7 provides a detailed illustration of this process, revealing the stable response characteristics of the sensor and its capability for accurate detection of trace  $\text{CH}_4$  and  $\text{NH}_3$ . These findings demonstrate that the developed sensor achieves high measurement accuracy and operational stability, thereby fulfilling the requirements for trace  $\text{CH}_4$  and  $\text{NH}_3$  detection in industrial and environmental monitoring applications.

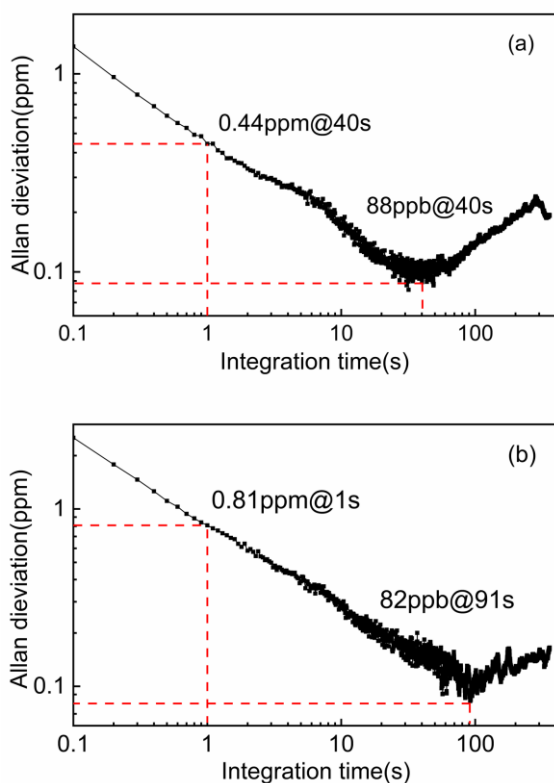


**Figure 6.** Allan variance of  $\text{NH}_3/\text{CH}_4$  under continuous measurement

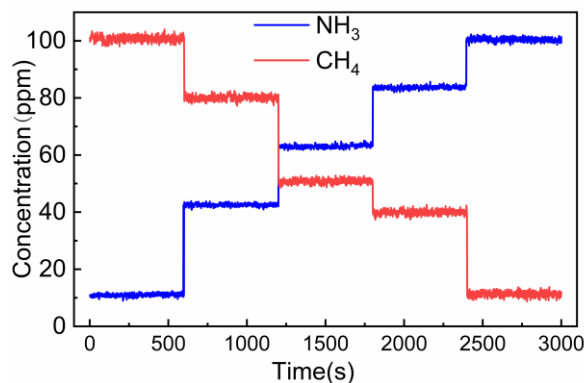


**Figure 7.** Continuous measurement results for trace  $\text{NH}_3/\text{CH}_4$  mixtures.

#### 4. Conclusions

This study presents the first sensor capable of simultaneously detecting trace levels of  $\text{CH}_4$  and  $\text{NH}_3$  in high-temperature, high-humidity environments. The innovative approach combines frequency division multiplexing with wavelength modulation spectroscopy by coupling 1512 nm and 1654 nm DFB lasers, thereby enabling quantitative, real-time measurements of trace  $\text{CH}_4$  and  $\text{NH}_3$  under challenging conditions:

- (1) A high-humidity trace mixed-gas configuration system was developed to accurately generate the desired target gas and water vapor concentrations. To verify the precision of the high-humidity setup, direct absorption spectroscopy (DAS) was employed to measure  $\text{H}_2\text{O}$  concentrations in the 10%–50% range, resulting in a maximum error of 3.5%. This confirms the reliability of the water vapor concentration control.
- (2) Subsequently, wavelength modulation spectroscopy (WMS) was used to detect trace concentrations of  $\text{CH}_4$  and  $\text{NH}_3$ . The sensor's performance was first evaluated in a high-temperature multipass gas cell, where temperature, pressure, and water vapor concentration were precisely controlled. Measurements of  $\text{CH}_4/\text{NH}_3/\text{N}_2$  mixtures with known concentrations and humidity levels yielded a detection limit of 88 ppb for  $\text{NH}_3$  (with an integration time of 40 s) and 82 ppb for  $\text{CH}_4$  (with an integration time of 91 s). Although the

$2f/1f$  signal peaks for both trace components are significantly affected when  $\text{H}_2\text{O}$  concentration exceeds 10%, a robust linear relationship with concentration is maintained.

(3) Experimental results demonstrate that the sensor exhibits excellent sensitivity, stability, and rapid response in real-time monitoring, satisfying the requirements for detecting trace fuel leakage in industrial combustion systems. In applications such as flue gas monitoring in  $\text{CH}_4\text{--NH}_3$  combustion systems and fuel leakage detection, the sensor provides precise measurements of trace  $\text{CH}_4$  and  $\text{NH}_3$ , offering critical data support for the safe, efficient, and low-emission operation of industrial combustion processes. In practical applications, the gas cell is operated at atmospheric pressure, and the sampling lines are insulated to maintain a constant temperature. Future research will explore the influence of temperature and pressure variations on the measurement of trace  $\text{NH}_3$  and  $\text{CH}_4$ , develop correction methods for such variations, and employ a calibration-free spectral model for concentration inversion to further enhance measurement reliability and accuracy in complex environments.

## 5. References

- [1] Xia J B, Zhu F, Zhang S S, et al. Probing greenhouse gases in turbulent atmosphere by long-range open-path wavelength modulation spectroscopy[J]. *Optics and Lasers in Engineering*, 2019, 117: 21-28.
- [2] Chao, X., Jeffries, J. B., and Hanson, R. K. 2012. Wavelength-modulation-spectroscopy for real-time, in situ NO detection in combustion gases with a  $5.2\mu\text{m}$  quantum-cascade laser, *Applied Physics B*, 106(4): 987-997.
- [3] Sun, P., Zhang, Z., Li, Z., et al. 2017. A study of two dimensional tomography reconstruction of temperature and gas concentration in a combustion field using TDLAS, *Applied Sciences*, 7(10): 990.
- [4] Chao, X., Jeffries, J. B., and Hanson, R. K. 2012. Wavelength-modulation-spectroscopy for real-time, in situ NO detection in combustion gases with a  $5.2\mu\text{m}$  quantum-cascade laser, *Applied Physics B*, 106(4): 987-997.
- [5] Gu, B., Zhang, L., Van Dingenen, R., et al. 2021. Abating ammonia is more cost-effective than nitrogen oxides for mitigating PM<sub>2.5</sub> air pollution, *Science*, 374(6568): 758-762.
- [6] Jha, R. K. 2022. Non-Dispersive Infrared Gas Sensing Technology: A Review, *IEEE Sensors Journal*, 22(1): 6-15.
- [7] Kira, O., Shaviv, A., and Dubowski, Y. 2019. Direct tracing of  $\text{NH}_3$  and  $\text{N}_2\text{O}$  emissions associated with urea fertilization approaches, using static incubation cells, *Science of the Total Environment*, 661: 75-85.
- [8] Moller, C., Wunscher, H., Frank, T., et al. 2021. Ammonia Sensors – Different Measurement Principles, *Proceedings of the 2021 Smart Systems Integration (SSI)*, IEEE, Zurich, Switzerland, 1: 1-4.
- [9] Ma, L., Wang, W., Zhou, C., et al. 2023. A laser absorption sensor for fuel slip monitoring in high-humidity flue gases from ammonia combustion, *Measurement Science and Technology*, 34(9): 094005.
- [10] Goldenstein, C. S., Spearrin, R. M., Jeffries, J. B., et al. 2017. Infrared laser-absorption sensing for combustion gases, *Progress in Energy and Combustion Science*, 60: 132-176.
- [11] Duan, K., Ji, Y., Wen, D., et al. 2023. Mid-infrared fiber-coupled laser absorption sensor for simultaneous  $\text{NH}_3$  and NO monitoring in flue gases, *Sensors and Actuators B: Chemical*, 374: 132805.
- [12] Guo, S., Li, J., Wei, Y., et al. 2024. A multi-laser

hybrid absorption sensor for simultaneous measurement of NH<sub>3</sub>, NO, and temperature in denitrification flue gas, *Infrared Physics & Technology*, 136: 105034.

[13] Guo, S., Li, Z., Liu, Z., et al. 2024. Simultaneous measurement of NH<sub>3</sub> and NO by mid-infrared tunable diode laser absorption spectroscopy based on machine-learning algorithms, *Measurement*, 234: 114858.

[14] Li, J., Zhang, C., Wei, Y., et al. 2020. In situ, portable and robust laser sensor for simultaneous measurement of ammonia, water vapor and temperature in denitrification processes of coal fired power plants, *Sensors and Actuators B: Chemical*, 305: 127533.

[15] Guo, X., Zheng, F., Li, C., et al. 2019. A portable sensor for in-situ measurement of ammonia based on near-infrared laser absorption spectroscopy, *Optics and Lasers in Engineering*, 115: 243-248